Catal Lett (2016) 146:2495–2503
DOI 10.1007/s10562-016-1878-3

Catalytic Properties of CeO_2-Supported $LaMnO_3$ for NO Oxidation

Hisahiro Einaga[1] · Wataru Yoshida[2] · Chanmin Lee[3] · Keisuke Kusaba[2]

Received: 15 July 2016 / Accepted: 24 September 2016 / Published online: 13 October 2016

Abstract CeO_2-supported $LaMnO_3$ perovskite oxides were prepared to study their catalytic properties in the oxidation of NO to NO_2. To prepare the catalyst and investigate the interaction between $LaMnO_3$ and CeO_2, two deposition methods were used. Extended X-ray absorption fine structure studies confirmed that perovskite oxide phases were formed on the CeO_2 support. Moreover, X-ray photoelectron spectroscopy and temperature-programmed reduction with H_2 studies revealed that the reduction temperatures for perovskite oxides and CeO_2 support decreased by the deposition followed by calcination at 650 °C, and that the interaction between the $LaMnO_3$ and CeO_2 support can be controlled by changing the preparation method. The $LaMnO_3/CeO_2$ catalyst in which $LaMnO_3$ was highly dispersed on CeO_2 exhibited higher NO oxidation activity than either $LaMnO_3$ or CeO_2. The thermal stability of the $LaMnO_3/CeO_2$ catalyst was compared with that of alumina-supported $LaMnO_3$ catalysts over 850–1050 °C.

Graphical Abstract

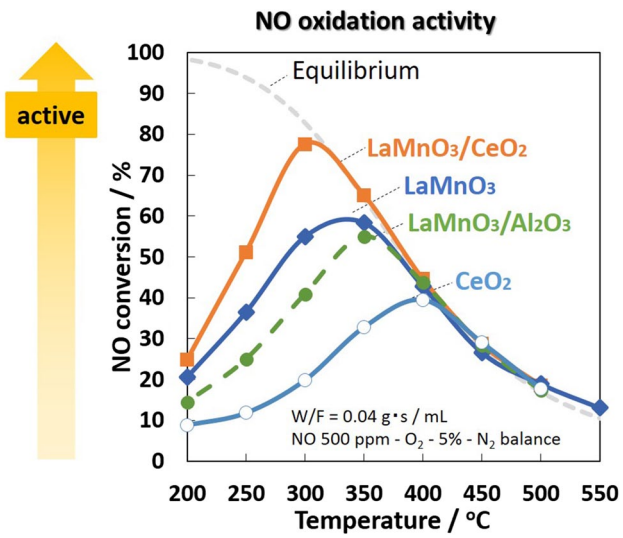

Keywords Supported catalysts · Perovskite oxides · CeO_2 · NO oxidation

1 Introduction

Automobile emission control technologies are attracting considerable attention due to the severe tightening of regulations and increasing vehicle production volumes. Catalytic NO oxidation is a critical process for the purification of diesel exhaust because the resulting NO_2 species is a key substance that promotes the oxidation of diesel soot and facilitates selective catalytic reduction and NOx storage under lean burn conditions. Supported Pt catalysts exhibit high activity in the oxidation of NO to NO_2 [1–3]. However, it is essential that the amount of noble metals used

✉ Hisahiro Einaga
einaga.hisahiro.399@m.kyushu-u.ac.jp

[1] Department of Energy and Material Sciences, Faculty of Engineering Sciences, Kyushu University, Kasuga, Fukuoka 816-8580, Japan

[2] Department of Molecular and Material Sciences, Interdisciplinary Graduate School of Engineering Sciences University, Kasuga, Fukuoka 816-8580, Japan

[3] Center of Advanced Instrumental Analysis, Kyushu University, Kasuga, Fukuoka 816-8580, Japan

in the catalysts be reduced or replaced by less expensive materials.

Perovskite-type mixed oxides, represented by a ABO_3-type formula, have been widely used as catalysts for oxidation processes [4–6]. Perovskite oxides are good substitute candidates for noble metal catalysts [7]. Perovskite oxides containing Mn [8–10] and Co [8, 11, 12] at the B site and La at the A site have been frequently used for the catalytic oxidation of NO to NO_2. In perovskite oxides, the A-site cations are partially substituted by Sr [13, 14] and Ce [15] and the B-site cations are partially substituted by other transition metals [16, 17]. Thus, one method for enhancing the catalytic activity of perovskite oxides is to substitute constituent metals and cations. Another method is to deposit them on supporting materials with a high surface area. To date, ZrO_2 [18, 19], Al_2O_3 [20], CeO_2 [21], and SiO_2-base mesoporous materials [22, 23] have been used to support perovskite deposition. The supported perovskite oxides reportedly exhibit high catalytic activity and thermal stability, which effectively offset the drawback of perovskite oxides—their low surface area.

We recently reported the selective deposition of the perovskite oxides $LaFeO_3$ and $LaMnO_3$ inside or outside the pore of γ-Al_2O_3 [24, 25]. These supported perovskite oxide catalysts exhibited higher activity and thermal stability than an alumina-supported Pt catalyst when the perovskite phases were deposited inside the alumina pore. These findings inspired us to investigate the effect of supporting materials on the catalytic properties of supported perovskite oxides. Here, we investigated the effect of depositing $LaMnO_3$ perovskite oxides onto a CeO_2 support on the catalytic properties of the oxidation of NO to NO_2. Because CeO_2 itself is active with respect to oxidation reactions, we anticipated that the combination of CeO_2 with perovskite oxide would improve the catalytic properties of the supported catalysts. We also investigated the effect of the deposition method on their catalytic properties and thermal stabilities, which were important factors when the catalysts were put into practical use for automobile emission control.

2 Experimental

2.1 Materials

The catalyst support CeO_2 (JRC-CEO-3; $S_{BET} = 72\ m^2\ g^{-1}$) was obtained from the Catalysis Society of Japan and was used after calcination at 650 °C for 5 h in air. γ-Al_2O_3 (JRC-ALO-8) was also used as a supporting material after the same treatment.

2.2 Preparation of $LaMnO_3/CeO_2$ Catalysts

Bulk $LaMnO_3$ perovskite oxides were prepared using the hydrolysis-precipitation method described in a previous paper [26]. The aqueous solution containing $La(NO_3)_3$ (Wako Pure Chem) and $Mn(NO_3)_2{\cdot}6H_2O$ (Wako Pure Chem) were slowly added to aqueous ammonia while vigorously stirring. The resulting precipitates were calcined at 650 °C for 5 h in air. The $LaMnO_3$ catalyst thus prepared has orthorhombic structure with the tolerance factor of 0.954. For the preparation of physical mixture of $LaMnO_3$ and CeO_2, 0.20 g of $LaMnO_3$ and 0.80 g of CeO_2 were ground with a mortar and pestle. The sample was denoted by $LaMnO_3$-MM.

To prepare CeO_2-supported $LaMnO_3$ ($LaMnO_3/CeO_2$) catalysts by the dry impregnation (DI) method, CeO_2 was impregnated with a mixed aqueous solution of metal nitrates in a quantity equal to 50–75 % pore volume of the CeO_2, followed by drying at 100 °C. The impregnation process was repeated until $LaMnO_3$ loading was increased to 20 wt%. The obtained samples were then calcined at 650–1050 °C for 5 h in air. The $LaMnO_3/CeO_2$ catalyst prepared by the DI method was denoted as $LaMnO_3/CeO_2$-DI.

$LaMnO_3/CeO_2$ catalysts were also prepared by a precipitation–deposition (PD) method. Hydroxide precursors of perovskite oxide were obtained by the hydrolysis–precipitation method described above. They were then mixed well in distilled water (300 mL) with CeO_2, followed by ultrasonication. Next, they were evaporated to dryness under vigorous stirring followed by grinding and calcination at 650 °C for 5 h in air. In this process, the loading level of perovskite phase after calcination depends on the water content of the hydroxide precursor. For the determination of $LaMnO_3$ loading on the CeO_2 support, therefore, the water content of the hydroxide precursor was measured by thermogravimetry (Shimadzu DTG-60) prior to the impregnation of the hydroxide precursor. The $LaMnO_3/CeO_2$ catalyst prepared by the PD method was denoted as $LaMnO_3/CeO_2$-PD.

2.3 Catalyst Characterization

The crystal structure of the catalysts was examined by X-ray diffraction (Rigaku Ultima IV) using CuKα radiation. The catalyst surface area was determined using Brunauer–Emmett–Teller (BET) plots obtained from the N_2 adsorption isotherms at 77 K (Quantachrome NOVA2000).

La K-edge extended X-ray absorption fine structure (EXAFS) spectra were taken with the photon factory advanced ring at the High Energy Accelerator Research Organization (NW-10A), with the storage ring operating at an energy of 6.5 GeV. Fourier transform-EXAFS spectra

were obtained from k^3-weighted EXAFS data [$k^3\chi(k)$] at 3.0–12.0 $Å^{-1}$. The coordination numbers (CNs), bond distances (R), Debye–Waller factor (σ^2), and energy shift (ΔE) were obtained using the theoretical backscattering amplitude and phase shift functions calculated by the program FEFF8 [27].

X-ray photoelectron spectroscopy (XPS) spectra were recorded using a Kratos AXIS-165 spectrometer with an Al Kα source. The binding energies were corrected using the value of 284.8 eV as an internal standard for the C 1s peak of the carbon species on the catalyst samples.

Temperature-programmed reduction with H_2 (H_2-TPR) was conducted with a BELCAT-30 catalyst analyzer (BEL JAPAN, Inc). The sample (0.050 g) was pretreated in an O_2 flow for 2 h at 823 K. In the H_2-TPR measurements, catalyst samples were heated at 10 °C/min.

2.4 Catalytic Activity Measurement

The catalytic oxidation of NO was performed using a fixed bed flow reaction system. Catalyst samples meshed at 250–750 μm were placed in the U-shaped glass reactor, which was connected to the system. The reaction gas, with a NO 500 ppm-O_2 5 %-N_2 balance composition, was fed to the reactor at 200–500 °C. In a typical reaction, the catalyst weighed 0.10 g and the gas flow was 150 mL/min ($W/F = 0.04$ g s mL^{-1}). The concentrations of NO and NO_2 were determined using a NOx analyzer (SHIMAZU NOA-7000). Prior to the reaction, the catalyst was heated in an O_2 flow at 550 °C. The oxidation of NO to NO_2 consists of both forward reaction ($NO + 1/2O_2 \rightarrow NO_2$) and backward reaction ($NO_2 \rightarrow NO + 1/2O_2$). Therefore, the steady-state activity was dominated by reaction equilibrium. The equilibrium curve for conversion of NO to NO_2 was calculated based on the van't Hoff Eqs. (1) and (2), where K_P, ΔH, R, T, p_{NO}, p_{NO_2}, and p_{O_2} were equilibrium constant expressed in terms of partial pressures of gases, the enthalpy of reaction, gas constant, reaction temperature, partial pressures of NO, NO_2, and O_2.

$$\frac{d \ln K_P}{dT} = \frac{\Delta H(T)}{RT^2} \tag{1}$$

$$K_P = \frac{p_{NO_2}}{p_{NO}\, p_{O_2}^{1/2}} \tag{2}$$

The reaction rate was obtained under conditions in which the NO conversion was linear with respect to the ratio of catalyst weight to gas flow rate.

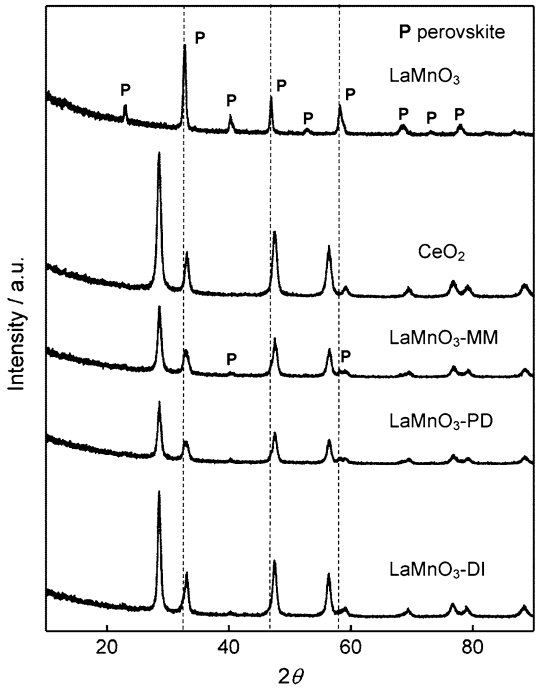

Fig. 1 XRD patterns of $LaMnO_3$ and $LaMnO_3/CeO_2$ catalysts prepared by different methods

Table 1 BET surface area and XPS analysis data of $LaMnO_3$ and $LaMnO_3/CeO_2$ catalysts

Catalyst	Surface area ($m^2\ g^{-1}$)	XPS analysis data		
		$Mn2p_{3/2}$	$Mn2p_{1/2}$	Mn/Ce intensity ratio
$LaMnO_3$	17	641.1	653.2	–
$LaMnO_3/CeO_2$-PD	68	641.1	653.3	0.071
$LaMnO_3/CeO_2$-DI	46	642.1	653.8	0.093

3 Results and Discussion

3.1 Structure of Catalysts

Figure 1 shows the XRD patterns of the CeO_2, $LaMnO_3$, and $LaMnO_3/CeO_2$ catalysts. The patterns of the CeO_2 support and $LaMnO_3/CeO_2$ combined were almost the same as those for the CeO_2 support alone, indicating that the structures of the CeO_2 support were unchanged after deposition and the post-heating treatment. The peaks due to the perovskite were detected for the physical mixture of $LaMnO_3$ and CeO_2 ($LaMnO_3$-MM) and the $LaMnO_3/CeO_2$ catalysts prepared by the PD. In contrast, perovskite phase was hardly detected for the $LaMnO_3/CeO_2$ catalyst prepared by the DI method, indicating that the $LaMnO_3$ perovskite phases were highly dispersed on the CeO_2 support.

The BET surface areas of the $LaMnO_3/CeO_2$ catalysts are listed in Table 1. The surface area of $LaMnO_3/CeO_2$ catalysts was lower than that of the CeO_2 support when the catalyst was prepared by the DI method, although the surface area of $LaMnO_3/CeO_2$ catalysts was much higher than that of the unsupported $LaMnO_3$ catalysts. It is noted that the surface area of the catalyst prepared by the PD method was nearly comparable to that of $LaMnO_3/CeO_2$-MM, whereas the $LaMnO_3/CeO_2$-DI catalysts have a much smaller surface area than those prepared by the PD method. This implies that the DI of perovskite oxides in the pores of the CeO_2 support promotes pore blockage during the calcination process.

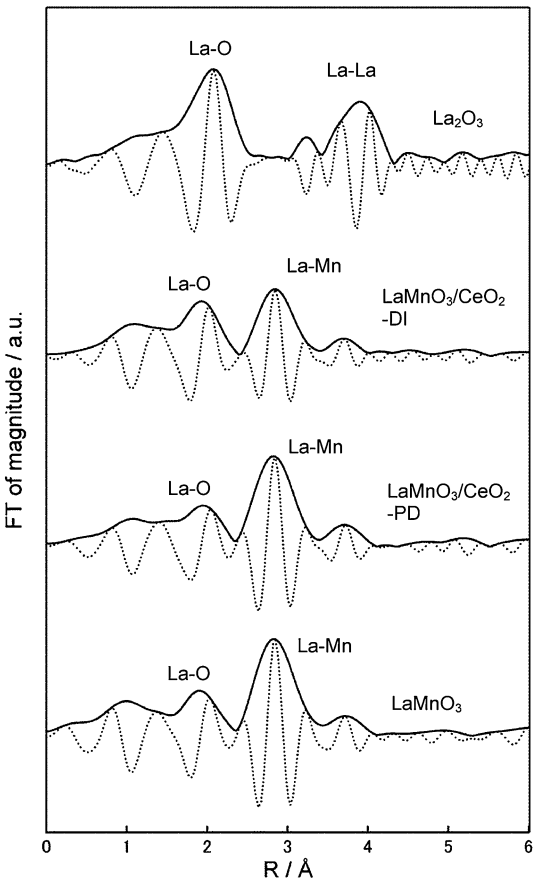

Fig. 2 La K-edge EXAFS spectra of $LaMnO_3/CeO_2$ catalysts and $LaMnO_3$

We studied the $LaMnO_3/CeO_2$ catalysts using EXAFS to investigate the structure of the mixed oxides present on the CeO_2 support. Figure 2 shows the La K-edge EXAFS spectra of $LaMnO_3/CeO_2$ catalysts along with those of the bulk $LaMnO_3$ and La single oxide (La_2O_3). The EXAFS spectrum of the bulk $LaMnO_3$ shows peaks at around 1.90 and 2.82 Å, which were identified as the La–O and La–Mn contributions of the perovskite structure, respectively. The perovskite oxides have 12-coordinated La–O bonds with different bond lengths in their first coordination shells (2.50–3.01 Å) and 8-coordinated La–Mn bonds in their second coordination shell (~3.37 Å). The first coordination shell cannot be fitted by a single La–O bond, indicating that the shell was composed of several La–O bonds of different bond lengths. The peak in the second coordination shell, however, can be fitted by a single La–Mn bond. The spectrum of La–single oxide indicates a La–O contribution at 2.09 Å and La–La contribution at 3.90 Å, which were much different from the peak positions of the bulk $LaMnO_3$.

The formation of a perovskite oxide phase for the $LaMnO_3/CeO_2$ catalysts was confirmed by the EXAFS studies. The $LaMnO_3/CeO_2$ catalysts also showed peaks at the same positions as those of the bulk $LaMnO_3$ catalyst. The absence of peaks due to the La–O and La–La contributions in the spectra of the $LaMnO_3/CeO_2$ catalyst shows that there were no impurity phases in the supported catalysts. The curve fitting results for the EXAFS spectra of the $LaMnO_3/CeO_2$ catalysts are listed in Table 2. The peak for the La–Mn contribution at 282 Å can be fitted well within the parameters of a single bond. The bond lengths for the La–Mn contribution were 3.340 Å and were not influenced by the deposition method. The values were consistent with those for the bulk $LaMnO_3$ perovskite oxides. The CN for the La–Mn contribution in $LaMnO_3/CeO_2$-PD was close to that for bulk $LaMnO_3$, whereas the CN value was much lower for $LaMnO_3/CeO_2$-DI. Thus, the CN value for the perovskite oxide phase depends on the preparation method. Since the CN value is related to the crystalline sizes of $LaMnO_3$, this implies that the sizes of the crystalline $LaMnO_3$ of the $LaMnO_3/CeO_2$ catalyst were smaller than those of the bulk $LaMnO_3$ catalyst and $LaMnO_3/CeO_2$-PD.

Figure 3 shows the XPS spectra of the $LaMnO_3/CeO_2$ catalysts and bulk $LaMnO_3$. In the XPS spectra ranges of

Table 2 EXAFS curve-fitting results for the $LaMnO_3$ and $LaMnO_3/CeO_2$ catalysts

Catalyst	La–Mn				
	CN	R (Å)	σ^2 (10^{-5} nm)	ΔE (eV)	R_f (%)
$LaMnO_3$	8.0	3.340 ± 0.010	3.60	−0.111	0.25
$LaMnO_3/CeO_2$-PD	7.9 ± 0.1	3.340 ± 0.010	4.36	−0.060	0.41
$LaMnO_3/CeO_2$-DI	5.6 ± 0.1	3.340 ± 0.010	4.49	−0.179	0.30

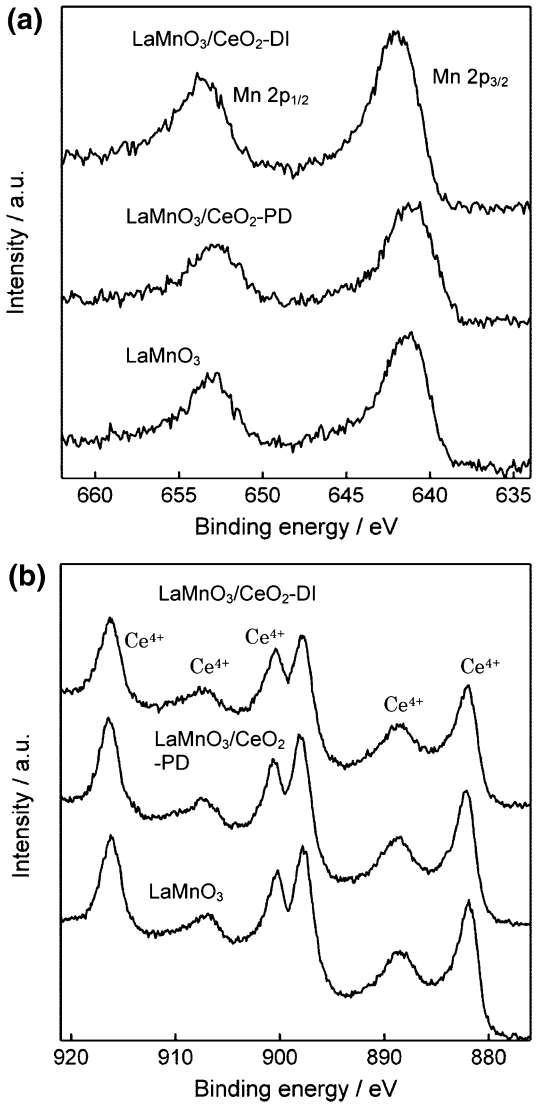

Fig. 3 XPS Mn 2p (**a**) and Ce 3d (**b**) spectra of $LaMnO_3/CeO_2$ catalysts and $LaMnO_3$

Mn 2p (635–660 eV), we observed the spin–orbit splitting of Mn $2p_{1/2}$ and Mn $2p_{3/2}$ signals (Fig. 4a). For $LaMnO_3$, the peak position of the Mn $2p_{3/2}$ signal was located at around 641.1 eV (Table 1) [28]. In the case of $LaMnO_3/CeO_2$ prepared by the PD method, we observed peaks for the Mn 2p signals at the same positions as those for the bulk $LaMnO_3$ catalyst. For $LaMnO_3/CeO_2$-DI, on the other hand, the Mn $2p_{3/2}$ peak was located in the range of 642.1 ± 0.1 eV, which was higher by 1.0 eV than that of bulk $LaMnO_3$. The full width at half maximum (FWHM) for the Mn $2p_{3/2}$ signal was comparable and larger than that for bulk $LaMnO_3$. This finding indicates that the oxidation state of Mn increased by the deposition of $LaMnO_3$ on CeO_2 by the DI method due to the strong interaction between $LaMnO_3$ and CeO_2.

In the Ce 3d region, peaks due to the presence of Ce $3d_{5/2}$ and Ce $3d_{3/2}$ were observed at 880–920 eV (Fig. 3b). These peaks mainly consisted of $3d_{5/2}$–$3d_{3/2}$ spin–orbit-split doublets characteristic of stoichiometric CeO_2 (Ce^{4+}) [29]. The peak positions for the $LaMnO_3/CeO_2$ catalysts were the same as those for bulk $LaMnO_3$, indicating that the surface states of the exposed Ce species were unaffected by the deposition of $LaMnO_3$.

Table 1 lists the calculated Mn/Ce intensity ratios for the $LaMnO_3/CeO_2$ catalysts. The value was higher for the catalyst prepared by the DI method than that prepared by the PD method. Because the XPS peak intensity ratio of metal-support elements is related to the dispersion of the metal oxides on the support [30], we can conclude that the dispersion of the $LaMnO_3$ phase was higher for $LaMnO_3/CeO_2$-DI. On the other hand, the XPS intensity ratio for $LaMnO_3/CeO_2$-PD was comparable to that for the mechanically mixed $LaMnO_3$-CeO_2.

Figure 4 shows TEM images of $LaMnO_3/CeO_2$-DI. The bright-field image (Fig. 2a) indicated that the catalyst was composed of particles with sizes of 10–20 nm. The DES mapping images (Fig. 2b–d) revealed that La and Mn were distributed over the whole particles of CeO_2 support. These observations confirm that $LaMnO_3$ particles were dispersed on the CeO_2 for $LaMnO_3/CeO_2$-DI.

3.2 H_2-TPR Studies

TPR of the $LaMnO_3/CeO_2$ catalysts by H_2 was carried out to further investigate the structure and reducibility of the catalysts. Figure 5 shows the H_2-TPR profiles for the $LaMnO_3/CeO_2$ catalysts, bulk $LaMnO_3$, and CeO_2. Here, the H_2 consumption was normalized to 0.2 g and 0.8 g for $LaMnO_3$ and CeO_2, respectively, whereas the value was normalized to 1.0 g for $LaMnO_3/CeO_2$ catalysts. For the bulk $LaMnO_3$ catalyst, H_2 consumption was observed in temperature ranges of 200–400 °C and 700–900 °C. The peak in the lower temperature range was ascribed to the reduction of Mn^{4+} to Mn^{3+}, and that in the higher temperature range to the reduction of Mn^{3+} to Mn^{2+} [10]. For the bulk CeO_2 support, reduction peaks were observed at 300–550 °C due to the reduction of surface Ce^{4+} and at higher temperatures due to the reduction of the bulk CeO_2 support [31]. In the case of $LaMnO_3/CeO_2$-PD, peaks appeared at around 136 °C. No peaks for the reduction of surface oxygen species on CeO_2 were observed, which had been observed at around 500 °C for bulk CeO_2. Quantitative analysis revealed that the amounts of H_2 consumed in the range of 50–550 °C in the $LaMnO_3/CeO_2$ catalyst were larger than the sum of the values consumed for the bulk catalysts (0.20 g-$LaMnO_3$ and 0.80 g-CeO_2). This reveals that the peak for the surface oxygen species on CeO_2 was shifted to a lower temperature by the $LaMnO_3$ deposition and indicates that the reactivity of the surface oxygen species on CeO_2 was improved. The peak maximum at around

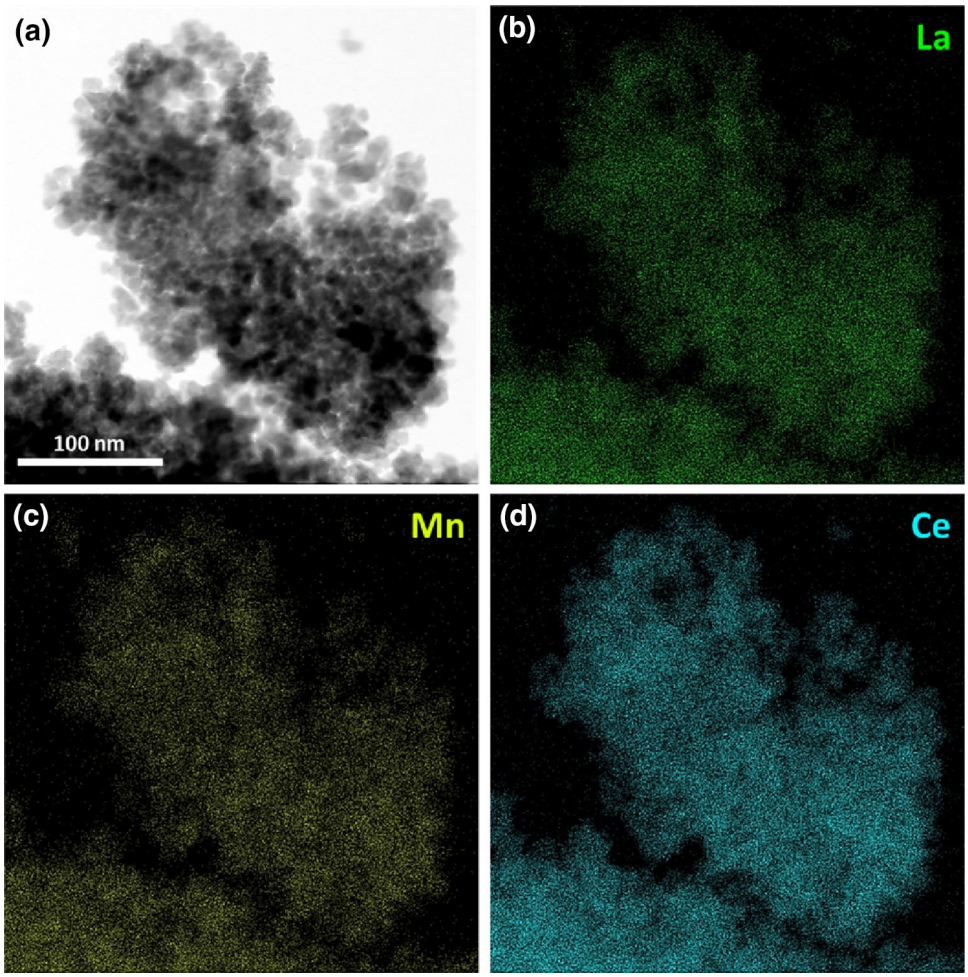

Fig. 4 TEM images of $LaMnO_3/CeO_2$-DI. Bright-field image (**a**), DES mapping image of La (**b**), Mn (**c**), and Ce (**d**)

800 °C was also slightly shifted to a lower temperature, indicating that the reactivity of the oxygen species on the catalysts and in the lattice were improved by the deposition of $LaMnO_3$ onto CeO_2.

In the case of $LaMnO_3/CeO_2$-DI, the peaks in the low temperature range (~400 °C) were much different from those of the bulk $LaMnO_3$ and $LaMnO_3/CeO_2$-PD: the H_2 consumption started in the same temperature range as that of $LaMnO_3/CeO_2$-PD, although the peak at 136 °C increased and the temperature of the reduction peak for Mn^{4+} to Mn^{3+} for $LaMnO_3$ was greatly lowered by the $LaMnO_3$ deposition on CeO_2. These findings indicate that, due to the strong interaction between $LaMnO_3$ and CeO_2, the reactivity of the oxygen species on the catalyst surface and in the lattice were improved by the deposition of $LaMnO_3$ onto CeO_2. The amount of H_2 consumed in the range of 50–550 °C was larger than that consumed with $LaMnO_3/CeO_2$-PD. These results also indicate that the amount of H_2 consumed is correlated with the dispersion of the perovskite oxides and that the interaction between $LaMnO_3$ and CeO_2 was controlled by changing the deposition method.

3.3 Catalytic Activity of CeO_2-Supported Perovskite Oxides

Figure 6 shows the catalytic activities of supported $LaMnO_3$ catalysts for NO oxidation in the temperature range of 200–500 °C, as compared with those for the bulk $LaMnO_3$ catalyst. For the purposes of comparison, the conversion curves for the equilibrium of NO oxidation ($NO + 1/2O_2 \rightleftharpoons NO_2$) were indicated. The $LaMnO_3/CeO_2$ catalyst exhibited steady-state activity and NO was quantitatively transformed to NO_2. The NO conversion increased with increased catalyst temperature up to 300 °C and decreased in the higher temperature range, following the equilibrium conversions. This indicates that the oxidation of NO to NO_2 is equilibrated with the backward reaction. Thus, the activity for NO oxidation was dominated by not only kinetics but also thermodynamics. The bulk $LaMnO_3$ catalyst exhibited lower NO conversion activity, with a maximum at 350 °C. The conversions of the CeO_2 catalyst were lower than those for the $LaMnO_3$ catalyst, with a maximum of 40 % conversions at 400 °C. A simple calculation shows that the activities of the $LaMnO_3/CeO_2$ catalyst cannot be explained in terms of

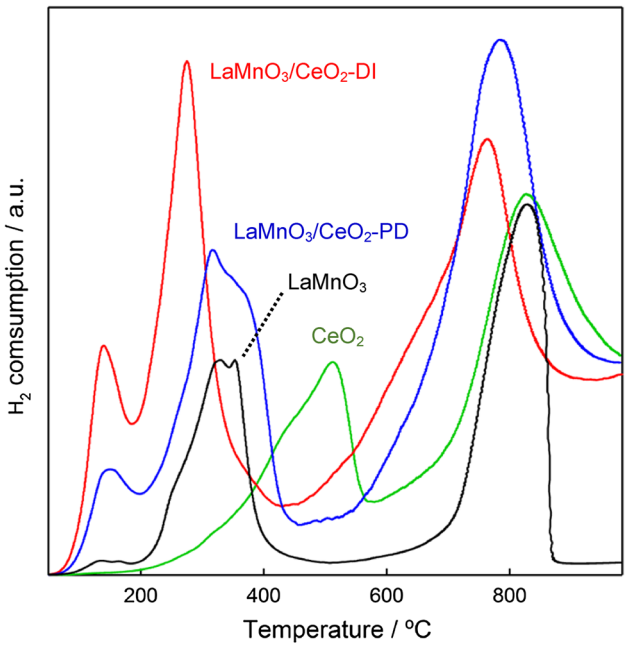

Fig. 5 H_2-TPR profiles of $LaMnO_3/CeO_2$ catalysts and $LaMnO_3$. Sample weight 0.050 g, gas composition 5 %H_2–N_2 balance, gas flow rate 30 mL/min, heating rate 10 °C/min

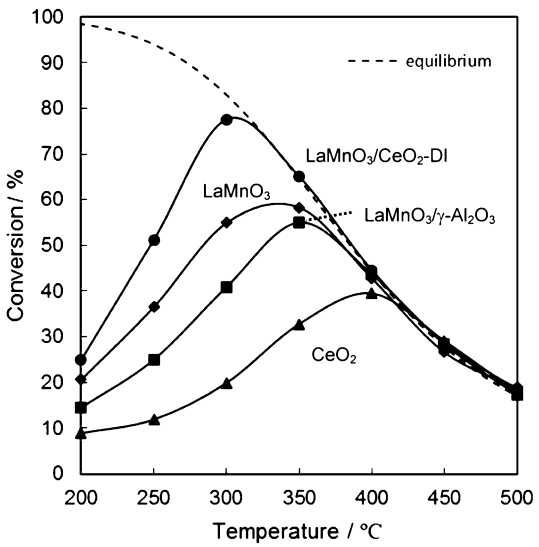

Fig. 6 Catalytic activities of $LaMnO_3/CeO_2$ catalysts and $LaMnO_3$ for oxidation of NO to NO_2. *Dashed line* refers to the dependence of equilibrium conversion reaction temperature. Reaction gas NO 500 ppm-O_2 5 %-N_2 balance, catalyst weight 0.10 g, the gas flow 150 mL/min (W/F = 0.04 g s/mL)

the activities of bulk $LaMnO_3$ and CeO_2: the physical mixing of $LaMnO_3$ and CeO_2 would correspond to much lower conversions. The $LaMnO_3/CeO_2$-DI exhibited higher activity than the catalyst prepared by the PD method, even though the latter had a larger surface area. The rates for NO oxidation at 200 °C for $LaMnO_3/CeO_2$-DI and $LaMnO_3/CeO_2$-PD were 7.4×10^{-6} and 3.3×10^{-6} mol g^{-1} min^{-1}, respectively. Thus, the high catalytic activity of $LaMnO_3/CeO_2$ prepared by the DI method was ascribed to the highly-dispersed $LaMnO_3$ species on CeO_2 and to the interaction between the catalytic materials. This result is probably due to the improved reactivity of the oxygen species of $LaMnO_3$ by deposition on CeO_2.

Because the $LaMnO_3/\gamma$-Al_2O_3 catalyst has shown high catalytic activity in propane oxidation [25], the results described above prompted us to compare the catalytic properties of the $LaMnO_3/CeO_2$ catalyst with those of a $LaMnO_3/\gamma$-Al_2O_3 catalyst prepared by the incipient wetness method, in which $LaMnO_3$ is deposited inside the alumina pores. The $LaMnO_3/CeO_2$ catalyst showed higher activity than the $LaMnO_3/\gamma$-Al_2O_3 catalyst (Fig. 6), even though the surface area of the $LaMnO_3/CeO_2$ catalyst was much smaller than that of the $LaMnO_3/\gamma$-Al_2O_3 catalyst (Table 1).

Lastly, we investigated the thermal stability of the $LaMnO_3/CeO_2$ catalyst for NO oxidation. The catalysts were heated at 850–1050 °C for 5 h in air and were again used for NO oxidation. As shown in Fig. 7, the X-ray diffraction (XRD) patterns of the $LaMnO_3/CeO_2$ catalyst exhibited the same CeO_2 structure as calcined catalysts when the catalyst was calcined at 850 °C. As the calcination temperature increased, the peak intensities increased and the FWHM decreased, which indicates the sintering of the supports. Correspondingly, the catalyst surface area significantly decreased: the surface areas of the $LaMnO_3/CeO_2$ catalysts after calcination at 850, 950, 1050 °C were 24, 11, 2 m^2/g, respectively. On the other hand, while the peaks for the perovskite oxides became more prominent, no other impurity phases were observed. It is worth noting that the calcination temperature in the range of 650–1050 °C was suitable for preparing bulk $LaMnO_3$ perovskite powder, and the supported $LaMnO_3$ phase was formed in the same temperature range.

The NO oxidation activity in the thermally treated $LaMnO_3/CeO_2$ catalyst decreased with increased catalyst calcination temperature. The maximum temperature for NO oxidation shifted to a higher temperature and the maximum conversion decreased: the conversions slightly decreased after the calcination temperatures reached 850–950 °C, and significantly decreased after the calcination temperature reached 1050 °C (Fig. 8). We also investigated the themal stability of $LaMnO_3/\gamma$-Al_2O_3 catalysts because they showed high stability for propane oxidation even when heated at high temperatures (650–1050 °C). Although the NO oxidation activity of the $LaMnO_3/\gamma$-Al_2O_3 catalyst decreased after themal treatment at temperatures between 850–1050 °C, the decrease in the NO oxidation activity of these catalyst was smaller than in the $LaMnO_3/CeO_2$ catalysts. This is probably due

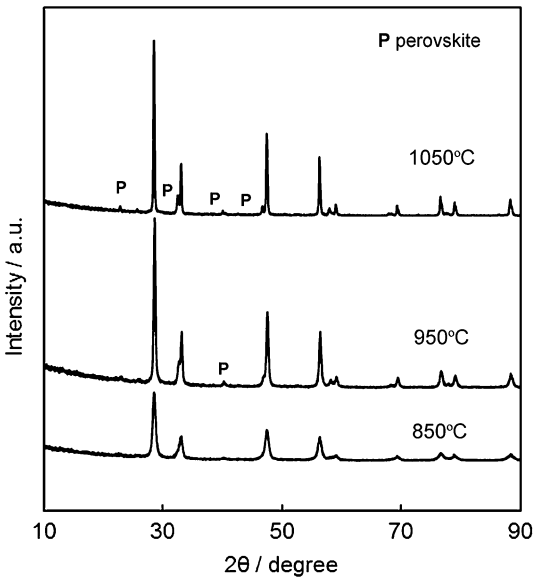

Fig. 7 XRD patterns of $LaMnO_3/CeO_2$-DI calcined at different temperatures

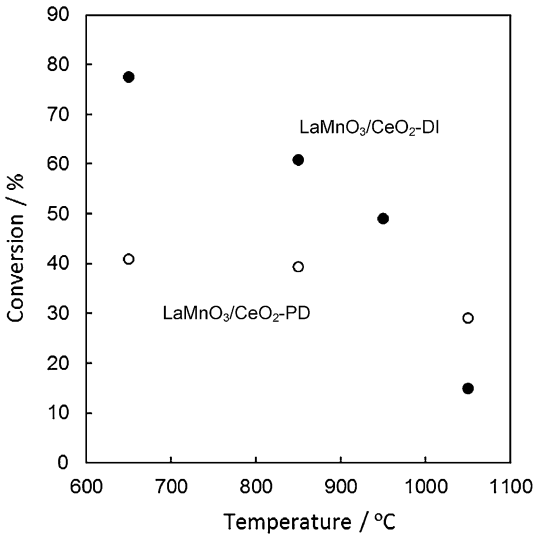

Fig. 8 Effect of heating treatment of $LaMnO_3/CeO_2$ and $LaMnO_3/\gamma\text{-}Al_2O_3$, catalysts on their NO oxidation activities. The reaction condition was the same as that in Fig. 6

to the improved stability of the perovskite phases when they were deposited inside the $\gamma\text{-}Al_2O_3$ pores. A comparison of the activity of the $LaMnO_3/CeO_2$ catalyst with that of $LaMnO_3/\gamma\text{-}Al_2O_3$, showed that the $LaMnO_3/CeO_2$ catalyst exhibited higher activity after calcination at 850 °C, whereas this activity dropped significantly after calcination at 1050 °C. This decrease in the catalyst activity was probably due to the decreased surface area and catalyst sintering. Thus, the $LaMnO_3/CeO_2$ catalyst is effective in promoting NO oxidation when calcined in the temperature range of 650–850 °C.

4 Conclusion

In this study, we prepared $LaMnO_3/CeO_2$ catalysts with different perovskite dispersions using four methods. The formation of $LaMnO_3$ perovskite phases was confirmed by EXAFS studies. The dispersion of $LaMnO_3$ perovskite oxide was evaluated by XPS. The $LaMnO_3/CeO_2$ catalyst prepared by the incipient wetness method exhibited higher NO oxidation activity although this catalyst has the smallest surface area. Based on the H_2-TPR study results, we propose that the higher level of activity may be ascribed to the strong interaction between the perovskite phase and the CeO_2 support. The supported catalyst was calcined in the temperature range of 650–1050 °C and then used for NO oxidation because thermal stability of the catalyst is important from a practical application perspective. The $LaMnO_3/CeO_2$ catalyst dry-impregnation method was more stable than $LaMnO_3/\gamma\text{-}Al_2O_3$ catalyst against heat treatment at the temperature lower than 950 °C.

References

1. Olsson L, Persson H, Fridell E, Skoglundh M, Andersson B (2001) J Phys Chem B 105:6895
2. Després J, Elsener M, Koebel M, Kröcher O (2004) Appl Catal B 50:73
3. Bhatia D, McCabe R W, Harnold M P, Balakotaiah V (2009) J Catal 266:106
4. Peña MA, Fierro JLG (2001) Chem Rev 101:1981
5. Zhu J, Li H, Zhong L, Xiao P, Xu X, Yang X, Zhao Z, Li J (2014) ACS Catal 4:2917
6. Royer S, Duprez D, Can F, Courtois X, Batiot-Dupeyrat C, Laassiri S, Alamdari (2014) Chem Rev 114:10292
7. Kim CH, Qi G, Dahlberg K, Li W (2010) Science 327:1624
8. Chen J, Shen M, Wang X, Wang J, Su Y, Zhao Z (2013) Catal Commun 37:105
9. Qi G, Li W (2012) Catal Today 184:72–77
10. Chen J, Shen M, Wang X, Qi G, Wang J, Li W (2013) Appl Catal B Environ 134–135:251
11. He X, Meng M, He J, Zou Z, Li X, Li Z, Jiang Z (2010) Catal Commun 12:165
12. Zhou C, Liu X, Wu C, Wen Y, Xue Y, Chen R, Zhang Z, Shan B, Yin H, Wang WG (2014) Phys Chem Chem Phys 16:5106
13. Choi SO, Penninger M, Kim CH, Schneider WF, Thompson LT (2013) ACS Catal 3:2719
14. Dong Y-H, Xian H, Lv J-L, Liu C, Guo L, Meng M, Tan Y-S, Tsubaki N, Li X-G (2014) Mater Chem Phys 143:578
15. Wen Y, Zhang C, He H, Yu Y, Teraoka Y (2007) Catal Today 126:400
16. Wang J, Su Y, Wang X, Chen J, Zhao Z, Shen M (2012) Catal Commun 25:106
17. Zhong S, Sun Y, Xin H, Yang C, Chen L, Li X (2015) Chem Eng J 275:351
18. Cimino S, Colonna S, De Rossi S, Faticanti M, Lisi L, Pettiti I, Porta P (2002) J Catal 205:309
19. Mizuno N, Fujii, Igarashi H, Misono M (1992) J Am Chem Soc 114:7151
20. Chagas CA, Toniolo FS, Magalhães RNSH, Schmal M (2012) Int J Hydrog Energy 37:5022

21. You R, Zhang Y, Liu D, Meng M, Jiang Z, Zhang S, Huang Y (2015) Chem Eng J 260:357
22. Nguyen SV, Szabo V, Trong On D, Kaliaguine S (2002) Micropor Mesopor Mater 54:51
23. Xiao P, Hong J, Wang T, Xu X, Yuan Y, Li J, Zhu J (2013) Catal Lett 143:887
24. Asada T, Kayama T, Kusaba H, Einaga H, Teraoka Y (2008) Catal Today 139:37
25. Asada T, Kusaba H, Einaga H, Teraoka Y (2015) Bull Chem Soc Jpn 88:1036
26. Teraoka Y, Kakebayashi H, Moriguchi I, Kagawa S (1991) Chem Lett 20:673
27. Ankudinov AL, Ravel B, Rehr JJ, Conradson SD (1998) Phys Rev 58:7565
28. Zampieri G, Abbate M, Prado F, Caneiro A, Morikawa E (2002) Physica B 320:51
29. Holgado JP, Munuera G, Espinós JP, González-Elipe AR (2000) Appl Surf Sci 158:164
30. Briggs D (1976) J Electron Spectrosc Relat Phenom 9:487
31. Bueno-López A (2014) Appl Catal B 146:1